The round turbulent jet in a cross-wind

By J. F. KEFFER AND W. D. BAINES
Department of Mechanical Engineering, University of Toronto, Toronto

(Received 20 July 1962)

The flow of a jet directed normal to a uniform, steady cross-wind is considered. Experimental results show that for various jet strengths, the position of the jet in space, when stretched by the ratio of jet to cross-wind momenta, is described by a single function. Exceptions exist at very low velocity ratios where a shift of the potential core is evident. A natural system of axes is used to define important directions of the flow. The integrated equation of motion along the primary jet flow direction is made dimensionless after the general method of Morton (1961) and a virtual source is defined for the flow. It is shown that a single functional behaviour of the axial jet velocity exists for various velocity ratios if the jet is considered to originate from this source. Lateral velocity profiles show a similarity when scaled by appropriate lengths and velocities but true self-preservation is not attained.

1. Introduction

The turbulent jet injected normal to a uniform, steady cross-wind is an example of a free turbulent shear flow. It is, however, inherently more complex than such cases as the jet entering a quiet medium or the wake at locations distant from a body. These possess geometric and kinematic properties which result in rather simple equations of motion, and by introducing physical concepts about the nature of free turbulence the distribution of mean velocity can be derived. There is thus a broad understanding of the flow pattern available for these simple free turbulent flows.

In this paper, the analysis of the jet in a cross-wind is based primarily on experimental observation of the flow pattern. Certain approximations are apparent, which when applied to the equations of motion, yield results similar to the simple cases. There are still important distinctions which prevent as complete a solution, however. The data, while not giving a comprehensive picture of the flow, should be useful in the solution of such practical problems as the discharge of waste gases from chimney stacks.

Velocity magnitude and direction were measured by hot-wire techniques at a large number of points covering the whole region influenced by the jet. Exploratory tests were conducted with photographs of smoke carried in the jet, (figure 1, plate 1). It is seen that there is a distinct edge to the jet. This is the typical boundary of a free turbulent flow described by Corrsin & Kistler (1955). Some form of statistical definition of the edge must be used for the analysis of mean velocities. The one chosen, which was introduced by Squire (1950),

defines the edge of the jet as the surface where the velocity excess above the external undisturbed flow, $(U-U_0)$, is 10% of the maximum excess (U_m-U_0), at a given cross-section. The location of the maximum velocity in the jet U_m, at succeeding positions downstream of the orifice defines the centre-line of the jet. It was noted that if cross-sections were taken perpendicular to the vector U_m, the direction of flow within the region bounded by the jet edge was essentially parallel to U_m. Following this line of maximum velocity, which is a stream-line, a jet is specified, analogous to the simple jet entering a quiet medium. Further measurements showed that relative to this centre-line, the lateral distribution of maximum mean velocity was an S-shaped curve. This was similar to the Gaussian distribution often used to describe the mean velocity distribution across a free jet.

The characteristic free turbulent flow which ultimately develops is a result of the mixing of two potential streams. At the source, the jet has an almost uniform velocity profile and a low turbulence intensity (compared to that which is subsequently generated). It thus may be assumed irrotational. Similarly, the cross-wind, outside the region of influence of the jet flow, is effectively irrotational. Immediately upon entering the cross-flow, the edges of the jet are subjected to intense shear stresses resulting from the velocity gradient between the jet and the cross-stream. In the free jet where the external flow velocity is zero, a uniform entrainment of the surrounding fluid occurs. The entrained fluid is accelerated as the jet spreads and the jet fluid is correspondingly decelerated. In the presence of the cross-wind this is complicated by the potential flow field surrounding the jet. The flow is decelerated at the upstream surface of the jet and creates a positive pressure region. The sides are subjected to a lateral shearing stress directed toward the rear. Jordinson (1958) has compared this flow to that around a porous cylinder with suction. Separation occurs at the rear and gives rise to a negative pressure region or wake. This initial stage of the flow is termed the zone of establishment and is similar to the free jet in that there is a constant maximum velocity, U_m, equal to the initial jet velocity U_j. This region extends for about five diameters for a free jet but is approximately one-half as long in the present case.

Once the potential core has been consumed and the biggest eddies in the flow are of the order of half the jet width, the continued lateral diffusion of jet momentum effects a decrease of the maximum velocity along the centre stream-line. This region, which is highly turbulent throughout the entire jet cross-section is called the zone of established flow, and possesses characteristics similar to the free jet. The external flow is affected very little by the presence of the jet and the static pressure and mean velocity can be considered constant.

At low ratios of jet to cross-wind velocity the potential core is deflected by the pressure field. The point at which the axial velocity begins to decay is thus shifted downwind. For velocity ratios greater than about four, the potential core is conical with the point approximately above the centre of the jet orifice. Hence the effect of the pressure forces and lateral shear is primarily to change the shape of the cross-section from the circle at the outlet to a characteristic kidney-shape at the end of the zone; see also Jordinson (1958) and Gordier (1959). The

sides of the jet possess less momentum than the centre because of the lateral mixing process and therefore are readily deflected. This effect is so severe that separation of the cross-flow from the edges of the jet occurs just behind the mid-section. A similar phenomena exists on a circular cylinder but with the jet the return flow in the centre of the wake is carried by the entrained fluid into the jet and so moves rapidly along the jet direction. The result is a pair of vortices attached to the jet which increase in strength throughout the zone of established flow. These are readily observed in smoke plumes from chimney stacks and have been previously described by Scorer (1958) and Turner (1960). Behind the vortices the cross-flow stream-lines become roughly parallel again but a large-scale turbulence persists as with the solid cylinder at a comparable Reynolds number.

With simple jets, entrainment occurs only by the spreading of the turbulent front. In the present case, this is augmented considerably by the action of the vortices which cause an internal circulation and hence large-scale mixing within the jet. In addition, some external fluid with small momentum is carried into the centre of the wake by the lateral shearing action. The total mass flux across the outside jet boundary is, therefore, significantly greater than in the free jet.

From observations and from considerations of the mechanics of the flow a general pattern of the established jet emerges. The strong mixing processes disperse the axial momentum over a steadily increasing area and thus the jet is continuously deflected downwind. The cross-sectional shape when viewed normal to the centre stream-line appears to remain approximately the same as that established at the end of the potential core, and it might be expected that mean velocity distributions taken along the lateral direction would show a similarity at successive cross-sections. Detailed measurements described later show this to be the case when the profiles are related by appropriate velocity and width scales. This however, is not a sufficient requirement for self-preservation and so the most general analysis of free turbulence cannot be applied to this flow. Observations of the motion far downstream lead to the conclusion that self-preservation is not approached in the limit. The mean velocity excess, $(U - U_0)$, decreases very rapidly along the jet axis but the rotational velocity of the vortices decreases at a rate, an order of magnitude less than this. Thus the limiting condition is a pair of counter-rotating turbulent line vortices moving with the speed of the cross-flow. For initial and intermediate stages of the jet, however, the mean velocity in the vortices is much smaller than the velocity excess and may be neglected in the calculation of mass and momentum fluxes. It would appear that the properties of the limiting condition would be more readily studied in a simpler geometric configuration where the vortices are generated directly.

2. Experimental technique

The experimental investigation was conducted in a low-speed air tunnel, 4 ft. by 8 ft. in cross-section with a test section 36 ft. long. The jet was discharged normal to the cross-wind from a $\frac{3}{8}$ in. diameter orifice with opening set flush into a circular plate. This plate, $\frac{1}{8}$ in. aluminium and 1 ft. in diameter with a carefully streamlined edge, was required to eliminate the effect of the boundary layer in

the tunnel and was placed 6 in. above the floor. An oil-vapour and nitrogen aerosol was used for the qualitative visual investigations. A compressed air supply was employed for the essential part of the experiment. A standard constant-current hot-wire anemometer was used to obtain the mean velocity contours and hence the mass and momentum fluxes along the direction of the jet flow. The wire was orientated to read the maximum velocity vector. Turbulence intensities were determined with an accurate random-signal voltmeter.

3. Analysis

The deflected jet

A system of axes, natural to the deflected jet is determined from experimental measurements and pertinent flow quantities are described along these principle axes (figure 2).

The ξ-axis is the centre stream-line of the jet flow.

The η-axis is defined by the locus of maximum velocity along lines of constant y in a plane perpendicular to the centre stream-line.

The ζ-axis is perpendicular to the ξ- and η-axes.

x, y and z are the vertical, lateral and longitudinal Cartesian co-ordinates relative to the cross-wind with origin at the jet source.

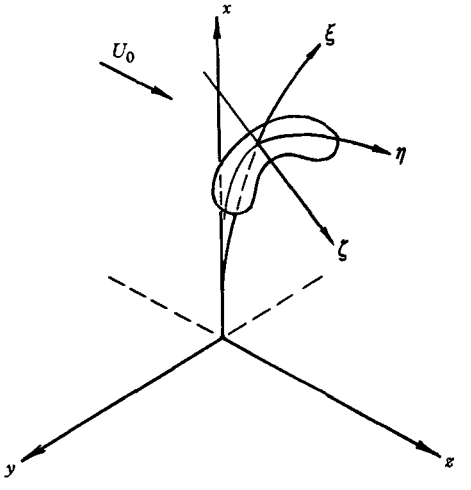

FIGURE 2. Natural system of axes for the jet.

Velocity ratios ($R = U_j/U_0$) of 4, 6 and 8 were chosen to cover a range that might normally be expected in practice. However, it was noted that at the lowest jet velocity ($R = 4$), the potential core appeared to be deflected by the strong pressure field set up around the jet by the cross-wind. The point at which the axial velocity began to decay thus did not remain along the $z = 0$ line. A further test at $R = 2$ verified this downwind shift. Results at a higher ratio, $R = 10$, were consistent with those previously found for $R = 6$ and 8 and the data are presented in figure 3.

In the absence of pressure gradients the deflexion of the jet depends inherently upon the amount of vertical momentum flux which it possesses relative to that of

the cross-wind, i.e. $R^2 = U_j^2/U_0^2$. For the larger velocity ratios this deflexion commences at the end of the zone of establishment where the turbulent mixing processes have extended across the entire jet. It is convenient to use this point, i.e. (x_0, z_0) (where $z_0 = 0$ for $R > 4$), as the origin for plotting the position of the jet in space. It is also convenient to divide the length dimensions by the orifice diameter d to give a pattern independent of the scale of the experiment. In

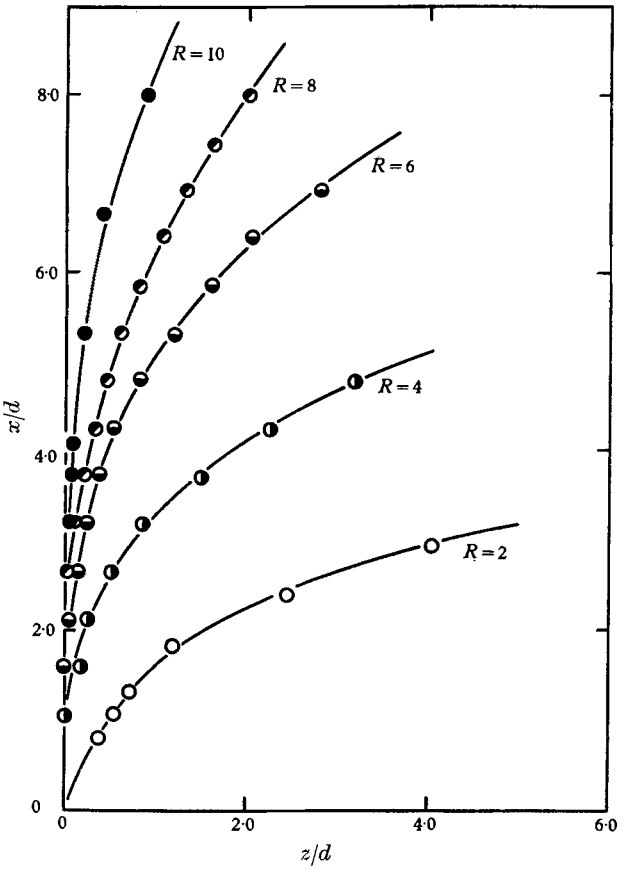

FIGURE 3. Location of jet centre-line.

addition, both x and z have been divided by R^2 the momentum-flux ratio. The reason for stretching both co-ordinates is deduced from the momentum equation for the direction ζ normal to the jet. The rate of change of deflexion angle is found to be the ratio of the ζ-direction momentum of the entrained flow and the ξ-momentum of the jet flow. Thus if these momenta are proportional to U_0^2 and U_j^2 respectively the deflexion angle at any time is inversely proportional to R^2. The co-ordinates are integrals of functions of jet velocity and deflexion angle and hence are also inversely proportional to R^2. Several approximations must be made to produce this simple proportionality and thus the results shown on figure 4 are somewhat surprising in the close fit to a single function for $R > 4$. A marked deviation is noted for $R = 2$ and 4 but these ratios must be considered as belonging

to different jet flows. The influence of the pressure field on the development region has resulted in the jet entering the established flow region at an angle less than 90° to the cross-wind. Observations with a smoke tracer show this behaviour (figure 1, plate 1). Furthermore, the jet appears to cling to the wall and thus the proximity of a solid surface may restrict the entrainment process.

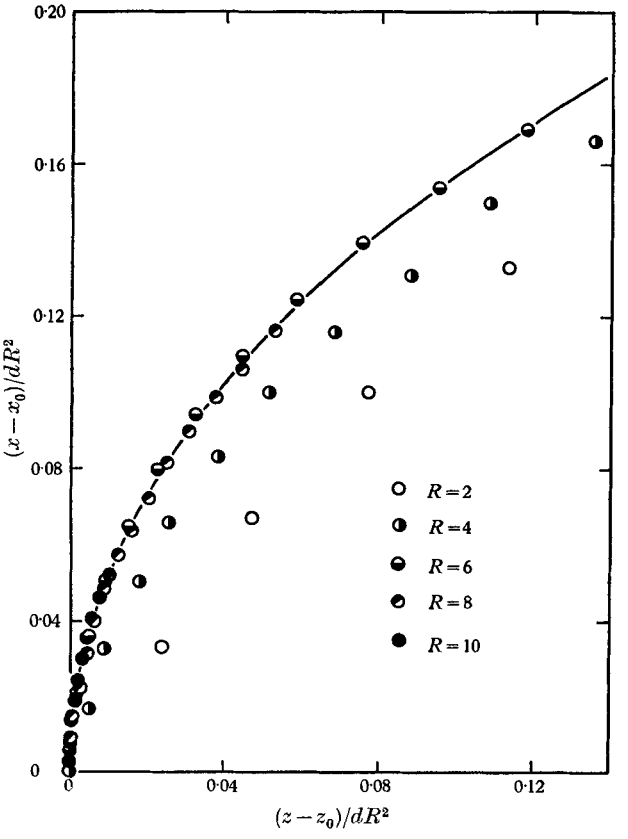

FIGURE 4. Jet centre-line as a function of momentum flux ratio, R^2.

The same process of reasoning and plotting of data can be applied to x and ξ along the centre stream-line and thus establish a relationship between the Cartesian and natural system of axes. Figure 5 is a plot of the appropriate parameters and as might be expected a single curve is obtained for the larger velocity ratios. No deviation is seen for the small ratios which indicates that the depth of penetration is not sensitive to the angle of the jet at the end of the potential core. More data are required at large values of $(\xi-\xi_0)/dR^2$ if this trend is to be verified for large R and the limiting conditions specified. These measurements are difficult to obtain because of the small velocity excess and the high turbulence intensity which makes the location of the velocity maximum uncertain. The value of x for very large ξ is of particular practical interest. In the literature the general implication is that there is a finite depth of penetration. This, however, is not consistent with the x-direction momentum equation. In the absence of pressure

forces the x-directed velocity must be finite for all z. The experimental data presented in figure 5 do not indicate an asymptotic behaviour but the range is too short. However, visual observations with a smoke trace show that at large distances ($z/d \approx 100$) the jet continues to rise.

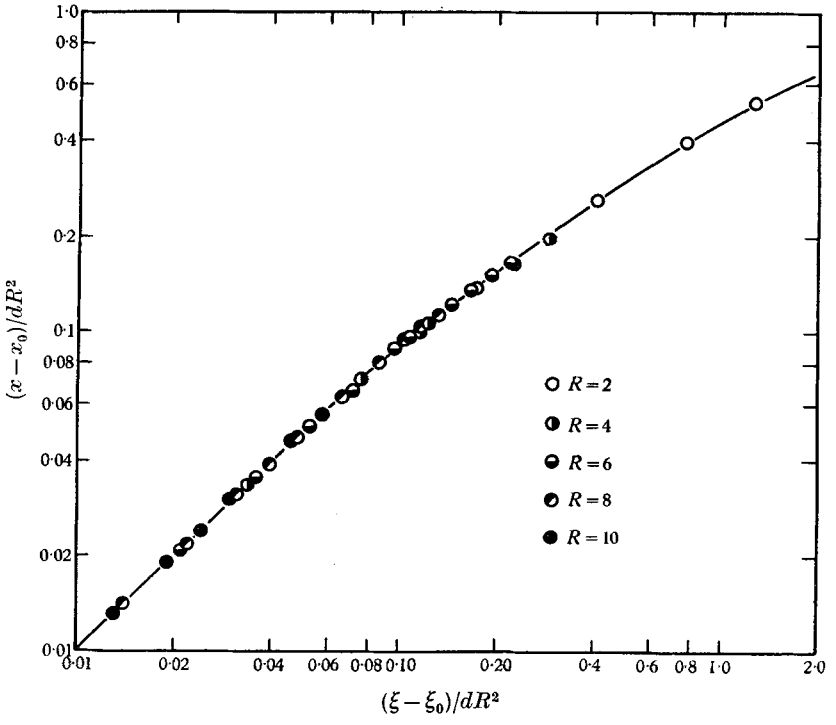

FIGURE 5. Penetration of the jet as a function of momentum flux ratio, R^2.

Equations of continuity and momentum

The experimental results indicate that the gradient of the linearizing factor in the ξ-direction is small with respect to the other terms in the equations. In addition, Reynolds number similarity (Townsend 1956) obtains since the Reynolds number of the flow is large enough for viscous effects to be ignored. With these assumptions the equation of continuity is readily obtained by equating the rate of change of mass flux across the jet-defined cross-section to the flow of mass into the jet across the outer edge per unit increment in ξ. The resulting equation is

$$\frac{1}{h_1}\frac{d}{d\xi}\int_A \rho U_1 dA = \oint_C \rho U_i dC \tag{1}$$

in which U_1 and h_1 are the velocity and linearizing factor for the ξ co-ordinate, U_i is the inflow velocity across the circumference C of the jet, and A is the cross-sectional area. The momentum equation for the ξ-direction is obtained in a similar manner by equating the rate of change of momentum flux in the jet to the momentum flux across the elemental circumferential area. In the notation used above this is

$$\frac{1}{h_1}\frac{d}{d\xi}\int_A \rho U_1^2 dA = \oint_C \rho(U_1 U_i)\, dC. \tag{2}$$

Entrainment

In simple free turbulent shear flows the eddies which effect the turbulent entrainment of exterior fluid are characterized by the relative velocities of the two fluid streams. In the present case, the mechanism of entrainment is complicated by the peculiar vortex formation at the rear of the jet. It would be expected therefore that the inflow is proportional more to the difference between jet velocity and cross-wind velocity, rather than the local parallel component of the cross-wind. Thus assuming that $U_i \sim (U_1 - U_0)$, where U_1 is some representative velocity within the jet, an entrainment coefficient can be defined as

$$E = U_i/(U_1 - U_0),$$

which for this particular flow is not necessarily a constant. It is realized that this formulation breaks down for $R = 1$ but this is not a serious defect because this case does not appear to exist in the form discussed above. For the jet and cross-wind velocities equal the zone of established flow would probably be a uniform flow in which $U_i = 0$. An alternative expression for E based on the vector velocity differences requires the inclusion of the local jet deflexion angle thus complicating the experimental analysis. Its use did not appear justified.

If mean velocity profiles are similar, the choice of a particular U_1 is quite arbitrary, since it need only represent the magnitude of the jet velocity. For simple jet flows, the centre-line velocity U_m is usually chosen. If integral relations are used, the averaged velocity over the jet cross-section $\overline{U_1}$, is conveniently employed. With this, the following expressions are defined,

$$v = \int_A U_1 dA = r^2 \overline{U_1}, \quad m = \int_A U_1^2 dA = r^2 \overline{U_1^2} = r^2 k (\overline{U_1})^2, \tag{3}$$

where k is a momentum coefficient, approximately unity in the present case, which occurs because of the non-uniformity of the velocity profiles, and r is an effective radius of the jet cross-section equal to $A^{\frac{1}{2}}$.

If the inflow velocity U_i is averaged over the circumference, the entrainment of mass and momentum fluxes can be simply expressed, as

$$\oint_C \rho U_i dC = sr\rho E(\overline{U_1} - U_0), \quad \oint_C \rho(U_1 U_i)\, dC = sr\rho E(\overline{U_1} - U_0)\, U_p,$$

where s is a shape factor for the jet cross-section equal to $A^{\frac{1}{2}}/C$, and the product $E(\overline{U_1} - U_0)\, U_p$ is the averaged contribution to the axial momentum flux of the jet resulting from the component of the external fluid parallel to the jet U_p which is entrained by the flow. It would be expected that the concomitant variables, E and U_p, are functions of ξ and R. It is necessary to determine their values experimentally.

Curvature of the jet axis is small for the high velocity ratios where similarity of profiles could be reasonably assumed. The linearizing factor, h_1, was calculated at the point of maximum curvature and found to be approximately 0·98. Consistent with the level of accuracy of the investigation, it was assumed unity at

all points along the axis. The statements of mass and momentum flux thus simplify to

$$d/d\xi(\rho v) = sr\rho E(\overline{U}_1 - U_0), \tag{4}$$

$$d/d\xi(\rho m) = sr\rho E(\overline{U_1} - U_0)\, U_p. \tag{5}$$

Dimensionless representation

The jet flow is completely turbulent by the time it reaches the end of the zone of establishment. It is convenient to refer to this point, ξ_0, as the *effective source* for the turbulent jet. Dimensionless values of mass and momentum flux are defined with respect to the flux values at this position, ρv_0 and ρm_0, and are correspondingly

$$V = \rho v/\rho v_0, \quad M = \rho m/\rho m_0.$$

The expression

$$d\xi = (v_0/sEm_0^{\frac{1}{2}})\, dX$$

is introduced to establish a dimensionless distance along the jet axis,

$$X = (sm_0^{\frac{1}{2}}/v_0)\int E\, d\xi,$$

where $E = E(\xi, R)$.

Following the general method of Morton (1961), substitution of the dimension less variables into the flux equations (4) and (5) yields

$$\frac{dV}{dX} = \frac{V}{(kM)^{\frac{1}{2}}}\left(\frac{M}{V} - B\right), \tag{6}$$

$$\frac{dM}{dX} = \frac{FV}{(kM)^{\frac{1}{2}}}\left(\frac{M}{V} - B\right), \tag{7}$$

where $B = kv_0 U_0/m_0$, a function of R only, and $F = v_0 U_p/m_0$. The solutions of these differential equations are subject to the boundary conditions at the effective source, $M = 1$, where $V = 1$. The dependence upon X can be eliminated by dividing equation (7) by (6), giving

$$dM/dV = F. \tag{8}$$

The functional behaviour of F is important to the solution but unfortunately cannot be predicted from the analysis. It is necessary to determine F experimentally.

Mass and momentum fluxes were measured for velocity ratios of 4, 6 and 8 and are plotted in figure 6 to show the relationship between M and V. It is seen that F, which is the slope of the (M, V)-function, is constant for each R and thus equation (8) can be integrated directly yielding the linear relation

$$M = 1 + F(V - 1). \tag{9}$$

The region $0 < V < 1$, represents the hypothetical flow for the fully turbulent jet and has no physical counterpart in the real flow. The point $V = 0$ defines a *virtual source* of zero mass flux but finite momentum flux, $(M)_{V=0} = 1 - F$, the value of which depends upon F, or, since $F = F(R)$, the velocity ratio of the jet. To examine the relationship between mass flux and position along the jet axis, equation (6) is rearranged as

$$\frac{dX}{dV} = \frac{(kM)^{\frac{1}{2}}}{M - BV},$$

which upon substitution of equation (9) becomes

$$\frac{dX}{dV} = \frac{k^{\frac{1}{2}}[1+F(V-1)]^{\frac{1}{2}}}{1-F+V(F-B)}, \tag{10}$$

with the appropriate boundary condition $V = 0$ at $X = 0$, the requirement of the virtual source.

Experimental measurements show that the term $V(F-B)$ is small with respect to the other terms in the equation for small values of V and may in the first approximation be neglected. In addition, $k^{\frac{1}{2}}$ is approximately unity. With these simplifications the relationship may be integrated directly, since $F = F(R)$ only, to give

$$X = \tfrac{2}{3}\{[1+F(V-1)]^{\frac{3}{2}} - (1-F)^{\frac{3}{2}}\}/F(1-F) \tag{11}$$

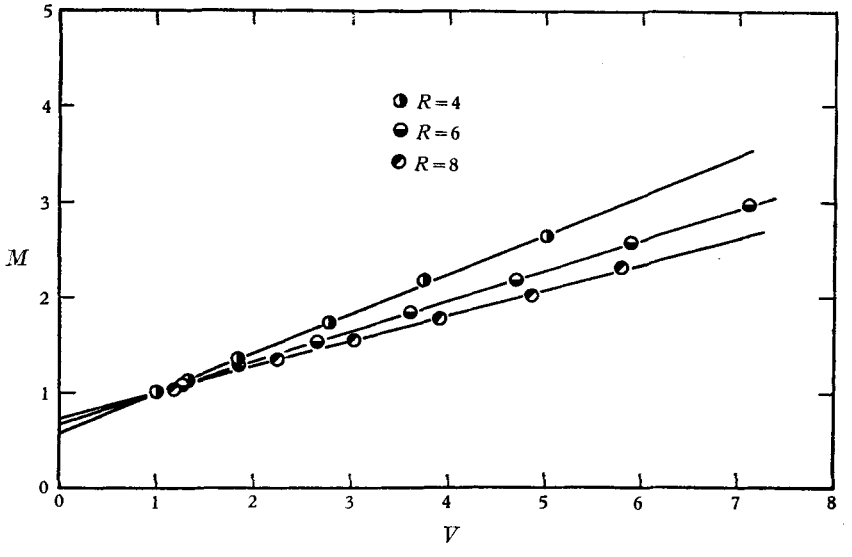

FIGURE 6. Mass-momentum flux diagram.

a result derived by Morton (1961) for the jet in a parallel stream. The dimensionless location of the effective source is obtained by letting $V = 1$, giving

$$X_0 = \tfrac{2}{3}[1-(1-F)^{\frac{3}{2}}]/F(1-F). \tag{12}$$

In terms of the entrainment coefficient E, the axial distance may be expressed as

$$X = \frac{sm_0^{\frac{1}{2}}}{v_0}\int_{\xi_V}^{\xi} E\,d\xi, \tag{13}$$

where ξ_V is the location of the virtual source. In particular the effective source is

$$X_0 = \frac{sm_0^{\frac{1}{2}}}{v_0}\int_{\xi_V}^{\xi_0} E\,d\xi, \tag{14}$$

and any position along the jet axis from the effective source is given by the definite integral

$$X - X_0 = \frac{sm_0^{\frac{1}{2}}}{v_0}\int_{\xi_0}^{\xi} E\,d\xi. \tag{15}$$

The entrainment function was determined from measurements of mass flux along the jet axis for the various velocity ratios. It is presented in figure 7 and is seen to depend upon ξ and R. Near the effective source, the magnitude of

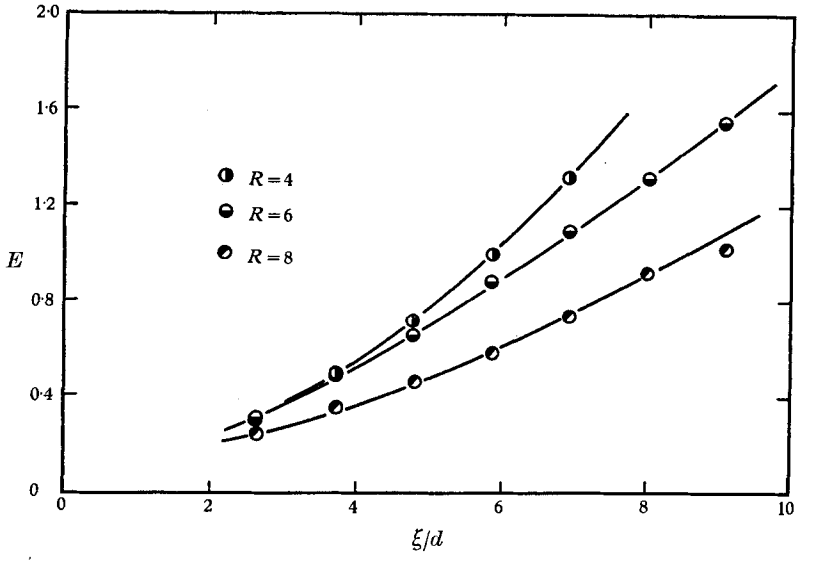

FIGURE 7. Entrainment coefficient as a function of position along jet axis.

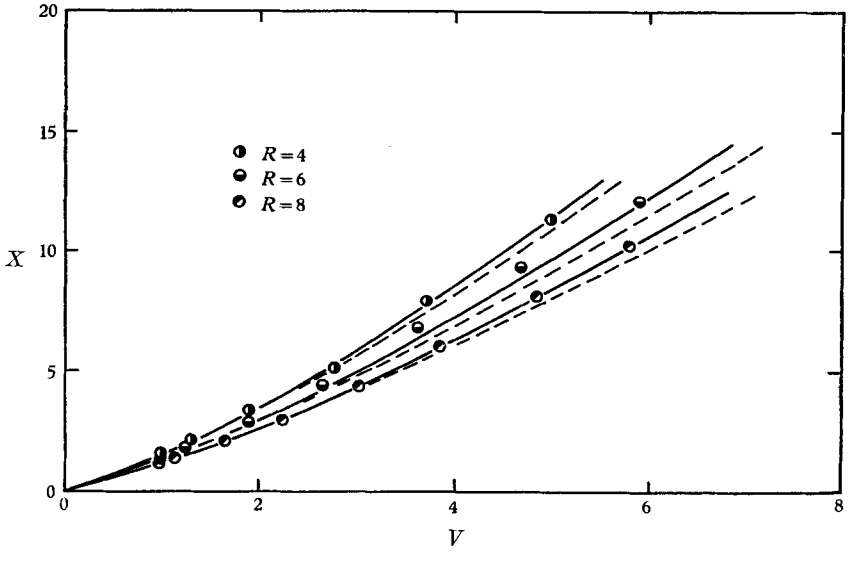

FIGURE 8. Relationship between dimensionless mass flux and dimensionless distance along the jet axis. – – – – Values calculated from equation (11).

E is of the same order as that found for the simple jet flows (Morton 1961). The function was integrated graphically to evaluate equation (15) and using the effective source ξ_0 as a matching point the results were compared to the approximate mathematical expression, equation (11), in figure 8. The agreement is

satisfactory at moderate values of V but tends to diverge for large V. There appears to be no single reason for this divergence.

The location of the virtual source may be estimated from equation (14). However, E cannot be measured in the region $\xi < \xi_0$ so it is necessary to extrapolate on figure 7. The value of ξ for which the definite integral is equal to X_0 (equation (12)), is the location of the virtual source in real space. This was determined for velocity ratios of 4, 6 and 8 and in each case the virtual source lay below the orifice. The distances were 1·87, 1·28 and 0·80 diameters respectively and appear to be in reasonable agreement with Ribner (1946) who found the virtual source for the jet in a parallel stream to lie 2·3 diameters upsteam from the discharge point.

4. Flow similarity in the jet

When related to the natural system of axes, the established jet flow appears to have many of the bulk characteristics of the free jet. The flow dimension in the direction of jet motion is at least an order of magnitude greater than the lateral dimension and this makes possible the usual boundary-layer type of assumption which neglects longitudinal diffusion with respect to lateral diffusion. Static pressure variations are small and the jet width increases monotonically in the downstream direction. It is natural to inquire if this resemblance to the free jet is retained in the detailed structure of the flow.

It is immediately evident that the flow is not completely self-preserving in the sense defined by Townsend (1956). The cross-wind would need to be an order of magnitude larger or smaller than the jet velocity excess for the equations of motion to be reducible to the appropriate form. Although the free jet meets these conditions for mean flow quantities, true self-preservation, as evidenced by similarity of the turbulence profiles, is not approached until twenty diameters from the source (Corrsin 1943). For the jet in a cross-wind, however, the flow at this distance is dominated by the twin vortices which prevents any asymptotic tendency toward similarity. Mean velocity distributions for the free jet are similar in the region of established flow when related to local characteristics, the centreline velocity and the half-velocity width. There is reason to expect that this might also be found for the deflected jet in intermediate regions where the vortices have not yet become the primary controlling influence on the flow. This is discussed below.

The similarity to be expected in the present situation should show an independence of the cross-wind velocity. Also, as with other free turbulent shear flows, Reynolds-number similarity is assumed, i.e. viscous effects can be neglected. Therefore, in the most general analysis, mean and turbulent velocity distributions are functions only of ξ/d, η/d, ζ/d and R. To achieve a universal representation of this flow, i.e. a similarity solution, independence of R is sought. Kinematic quantities should thus be able to be described only in terms of a local length scale (say the half-velocity width) and a local velocity scale. For the latter, it would appear that the velocity excess above the cross-wind is the most significant since at large distances downstream the jet velocity approaches U_0. It might be expected that from a consideration of the jet purely as a momentum

phenomena, the velocity excess could be defined in terms of the local parallel component of the cross-wind. However, the normal component as well contributes significantly to the jet spreading and must be included. The simplest combination of these components is of course U_0, hence $(U - U_0)$ is the most reasonable choice. Experimental results indicate that similarity is indeed found only for $(U - U_0)$.

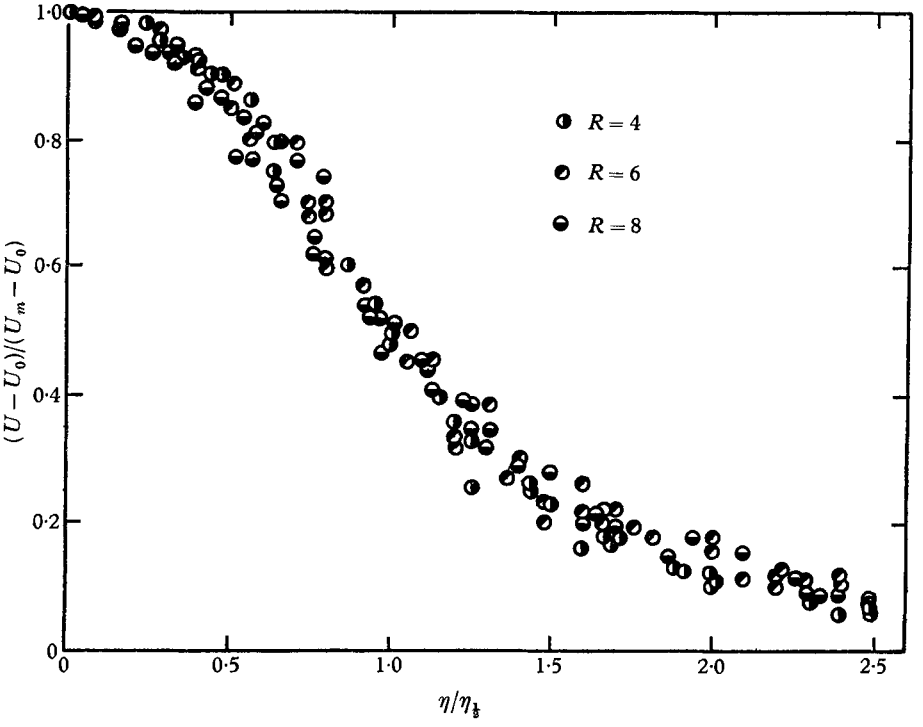

FIGURE 9. Lateral distribution of jet velocity.

Figure 9 presents the velocity distribution along the lateral direction (the η-axis) at successive ξ positions in the zone of established flow. When related in terms of the characteristic velocity, $(U_m - U_0)$, which is the velocity excess at the jet centre, and a characteristic length $\eta_{\frac{1}{2}}$, which is the point where $(U - U_0)$ is one-half $(U_m - U_0)$, a single S-shaped curve is obtained for the velocity ratios 4, 6 and 8. A considerable scatter of the points is evident but no consistent deviation exists. The axial component of turbulence intensity, u_1', was measured at one station $\xi'/d = 5{\cdot}6$ (figure 10). It is seen, however, that these profiles, although having a common shape, are not independent of the velocity ratio as are the mean velocity profiles.

The characteristic velocity and length scales should be single functions of the distance along the jet if the flow is to exhibit self-preservation of the mean velocity profiles. Logically, this distance should be that measured from the virtual source, ξ'/d. On this basis, figures 11 and 12 indicate that the velocity excess, made dimensionless by dividing by the maximum excess, $(U_j - U_0)$, and the jet width at the half-velocity point, have the required behaviour in that both quantities are independent of the velocity ratio. (It is seen from figure 11 that the decay

of $(U_m - U_0)$ is a function of R when plotted from the orifice outlet. This can also be inferred for the jet spread in figure 12.) These results are analogous to those of the free jet and are consistent with the idea of self-preservation which is implied by the single curve in figure 9. The velocity excess, however, decreases much more

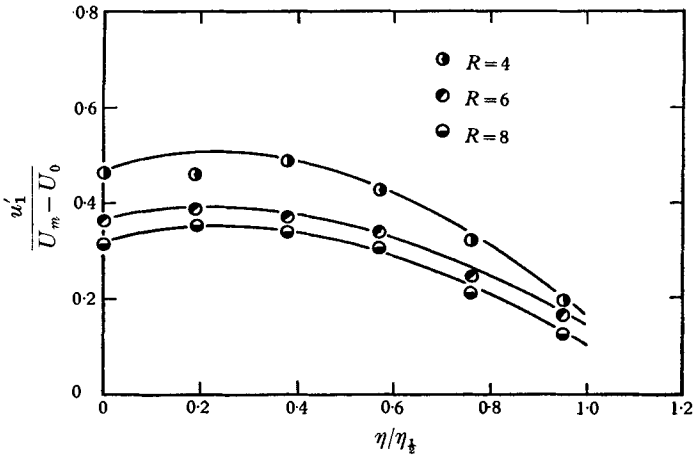

FIGURE 10. Lateral distribution of axial turbulence intensity at $\xi'/d = 5{\cdot}6$.

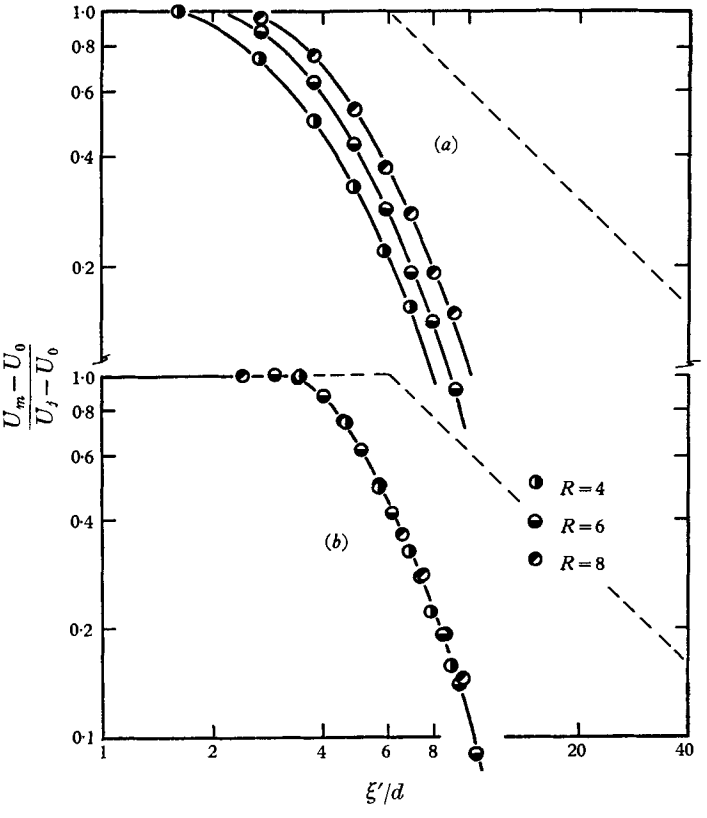

FIGURE 11. Decay of jet axial velocity compared to free jet: (*a*) plotted from orifice outlet; (*b*) plotted from virtual source. – – – – Free-jet data of Albertson *et al.* (1950).

rapidly than for the free jet results of Albertson, Dai, Jenson & Rouse (1950) and the rate of decrease increases with distance away from the source. This is because the entrainment is augmented by secondary effects, primarily the twin vortices, which do not exist in the free jet. The lateral spreading of the flow, which has the same general trend as that for the free jet, does not appear to be affected.

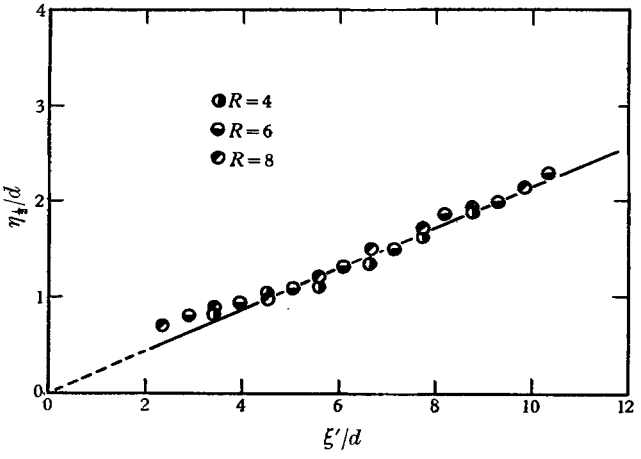

FIGURE 12. Lateral spread of jet determined at the half velocity point, i.e. $(U-U_0)/(U_m-U_0) = \frac{1}{2}$.

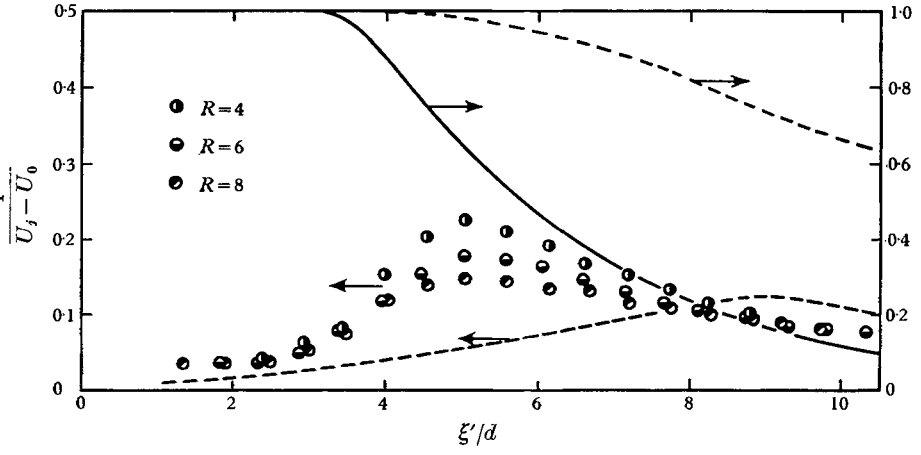

FIGURE 13. Turbulence intensities along jet axis compared to the free jet. – – – – Free-jet data of Corrsin & Uberoi (1950).

This is not surprising since the vortices have been observed to increase in diameter at a much smaller rate than the spread of a free jet.

Since the effective source is the point at which the axial velocity begins to decay, the distance between the virtual and effective sources should be approximately constant if the jet is to display a similar kinematic behaviour for the various velocity ratios. The data verify this since for $R = 4$, 6 and 8, the values are 3·46, 3·20 and 3·10 diameters, respectively. The decreasing size of this distance with increasing R may indicate that similarity with velocity ratio may not be found for a very large range of velocity ratios.

The distribution of turbulence intensity along the jet axis also reflects the effects of the more intensive entrainment processes. In figure 13 the intensity of axial turbulence, u_1', is plotted against the distance from the virtual source, ξ'/d. Free-jet measurements are included for comparison. The maximum turbulence intensity occurs at approximately the same position (relative to the mean velocity) in both cases but is considerably larger in magnitude for the jet in a cross-wind. A variation in intensity with jet strength, moreover, indicates that the similarity observed for the mean velocity, is not retained in the fine structure of the flow.

5. Discussion

All of the experimental evidence indicates that the jet flow displays similarity along the natural system of axes. This conclusion may be of more extensive significance than for the flow considered here. Other cases of free turbulence in which symmetry is lacking might be analysed with conventional methods by the proper choice of co-ordinates. The measurements were not carried out at a sufficient distance to show if the flow approaches a self-preserving form in the limit, i.e. unique local distribution of turbulent intensity and Reynolds stresses based on $(U_m - U_0)$. The available equipment did not allow the measurement of the small velocity excess and Reynolds stress. It is the author's opinion that since the line vortices are the dominant mixing agents they should be studied in a simpler and more controllable configuration. The vortices exert a major effect on the flow and thus mean vorticity can be expected to play an important part in other free turbulent flows.

The experimental study reported in this paper was supported by a grant from the University of Toronto.

REFERENCES

ALBERTSON, M. L., DAI, Y. B., JENSEN, R. A. & ROUSE, H. 1950 Diffusion of submerged jets. *Trans. A.S.C.E.* **115**, 639.

CORRSIN, S. 1943 Investigation of flow in an axially symmetrical heated jet of air. *N.A.C.A. War Rep.* W94.

CORRSIN, S. & KISTLER, A. L. 1955 Free-stream boundaries of turbulent flows. *N.A.C.A. Rep.* no. 1244.

CORRSIN, S. & UBEROI, M. S. 1950 Further experiments on the flow and heat transfer in a heated turbulent air jet. *N.A.C.A. Rep.* no. 998.

GORDIER, R. L. 1959 Studies on fluid jets discharging normally into moving liquid. St Anthony Falls Hyd. Lab., University of Minnesota, *Tech. Paper*, no. 28, Series B.

JORDINSON, R. 1958 Flow in a jet directed normal to the wind. *Aero. Res. Council, R & M*, no. 3074.

MORTON, B. R. 1961 On a momentum-mass flux diagram for turbulent jets, plumes and wakes. *J. Fluid Mech.* **10**, 101.

RIBNER, H. S. 1946 Field of flow about a jet and effect of jets on stability of jet-propelled airplanes. *N.A.C.A. War Rep.* L 213.

SCORER, R. S. 1958 *Natural Aerodynamics.* Pergamon Press.

SQUIRE, H. B. 1950 Jet flow and its effect on aircraft. *Aircraft Engng*, **22**, 62.

TOWNSEND, A. A. 1956 *The structure of Turbulent Shear Flow.* Cambridge University Press.

TURNER, J. S. 1960 A comparison between buoyant vortex rings and vortex pairs. *J. Fluid Mech.* **7**, 419.

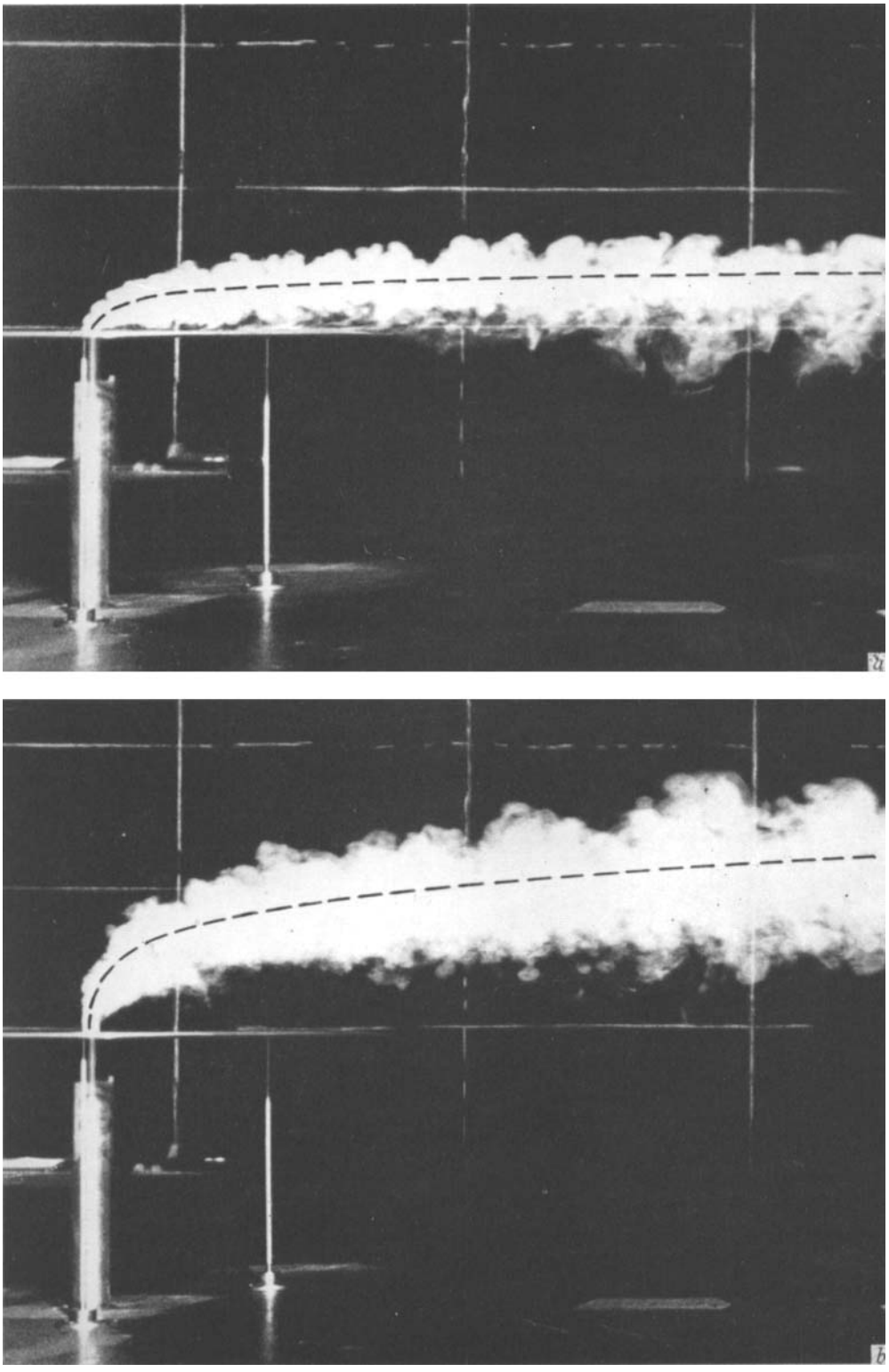

FIGURE 1. Photographs of jet in a cross-wind at 1/1300 sec exposure.
(*a*) $U_0 = 5$ ft./sec; $R = 2$. (*b*) $U_0 = 5$ ft./sec; $R = 8$. – – – –, Jet axis.

KEFFER AND BAINES

(*Facing p.* 496)